SUPPLEMENTAL FIGURES

Figure S1 (related to Figure 1). Highly efficient cortical organoid differentiation derived from multiple hES and iPS cell lines.

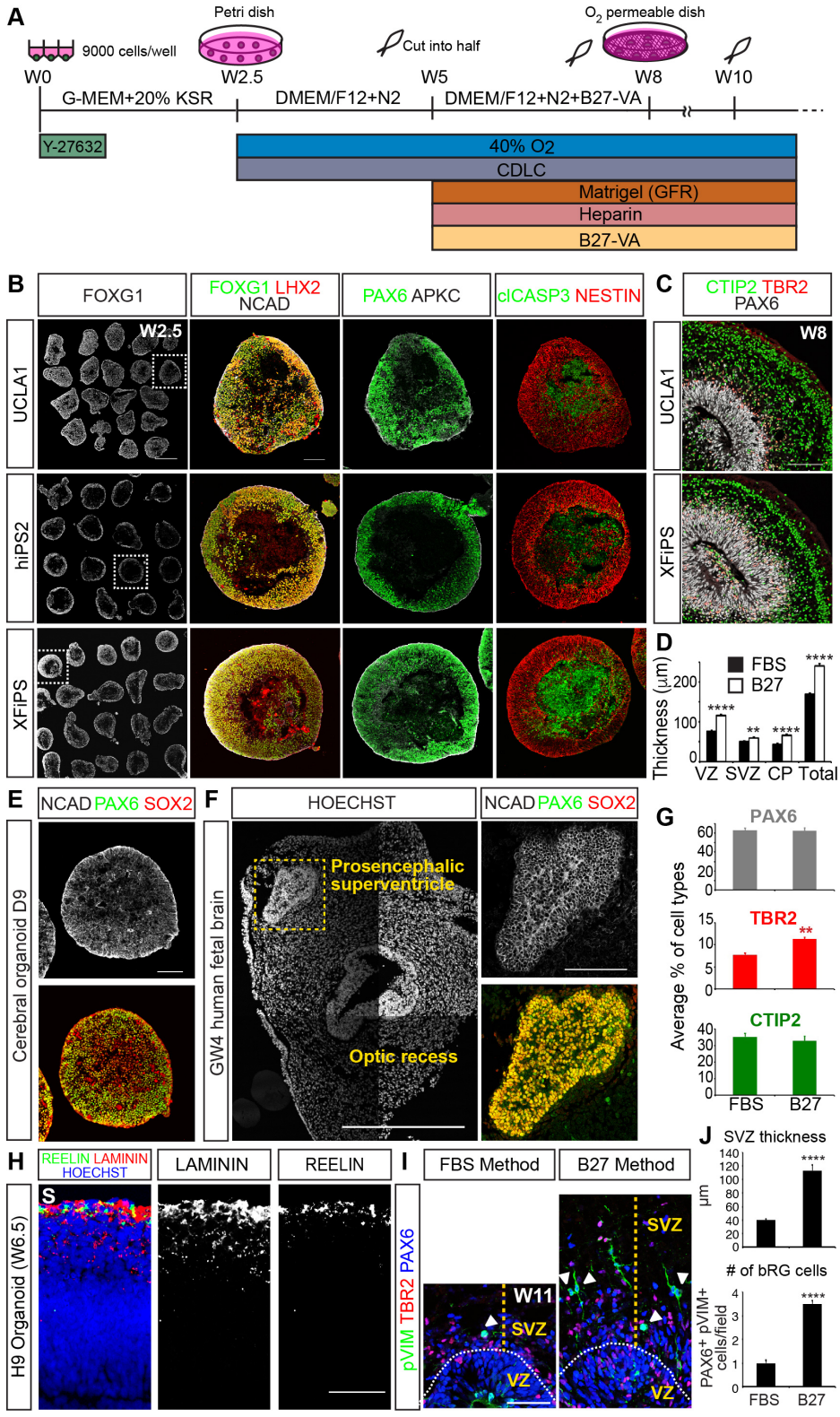

(**A**) Schematic of organoid differentiation protocol. (**B**) W2.5-cerebral organoids derived from three hPS cell lines and immunostained for telencephalic (FOXG1/LHX2/PAX6), progenitor (NESTIN), apical membrane (APKC/NCAD), and cell death (clCASP3) markers. (**C**) W8-cerebral organoids from UCLA1 and XFiPS lines, demonstrating laminar organization of the $PAX6^+$ VZ, $TBR2^+$ SVZ, and $CTIP2^+$ CP regions. (**D/G**) Continued from (Fig. 1D-E). FBS versus B27 media components. Average thickness of cortical zones. Average percentage of cells positive for markers out of total cells per field. Data are represented as mean ± SEM. (**E**) Early neuroectodermal organoids at D9 with relatively uniform expression of progenitor markers NCAD, PAX6, and SOX2. (**F**) Sagittal section of GW4 human prospective forebrain region with NCAD, PAX6, and SOX2 markers. (**H**) W6.5-cerebral organoids immunostained for basement membrane (LAMININ) and Cajal-Retzius cells (REELIN). (**I-J**) Comparison of SVZ thickness and bRG cell number in FBS vs B27 media components. Data are represented as mean ± SEM. Scale bars: B, F left, 500 μm; B right, C, E, F right, 100 μm; H, I 50 μm.

Figure S2 (related to Figure 1). Comparison of organoid differentiation methods.

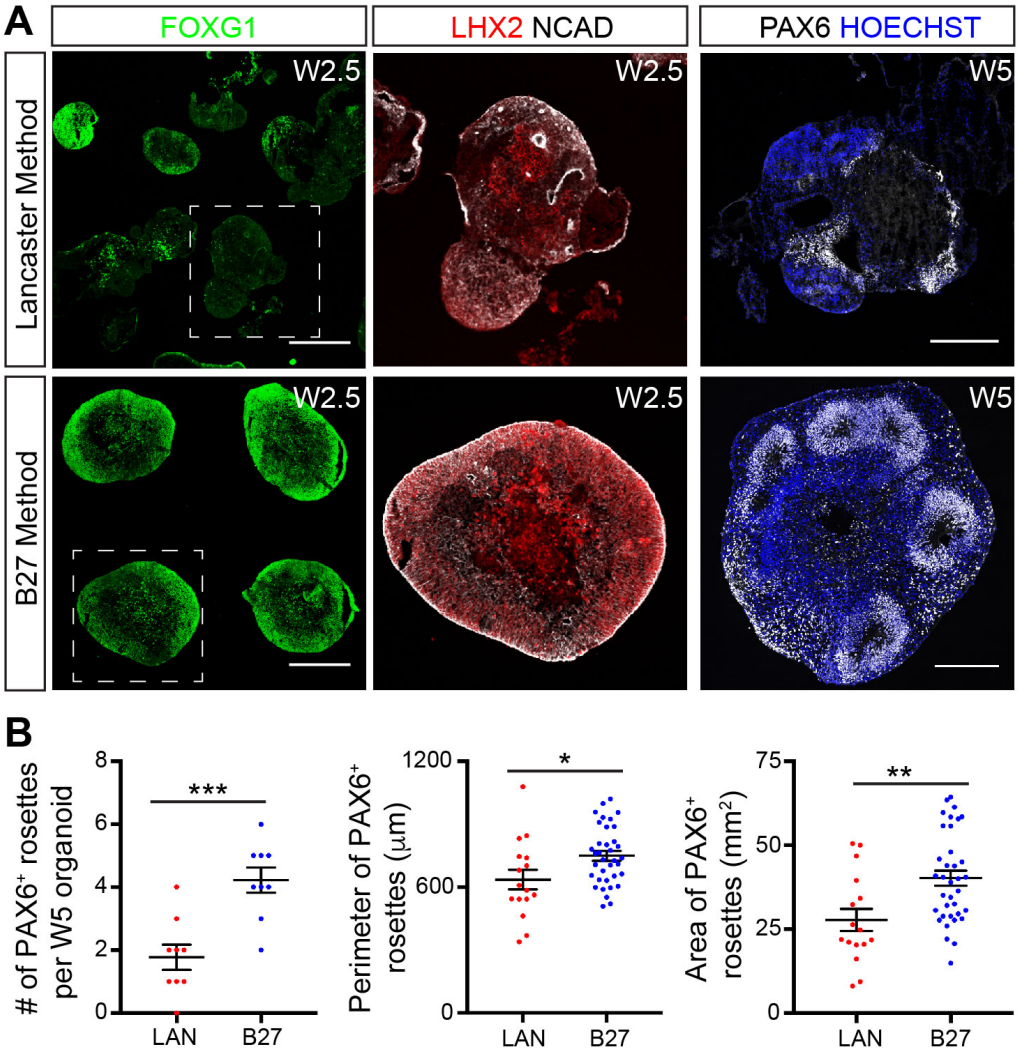

(**A**) H9 hESC differentiated using Lancaster et al. *Nature* 2013 or B27 method (described in Fig. S1A). W2.5 and W5 organoids stained for forebrain marker (FOXG1), cortical progenitor marker (LHX2), neuroepithelial marker (N-Cadherin), and progenitor marker (PAX6). (**B**) Quantitative analysis of $PAX6^+$ neural structures. Data are represented as mean ± SEM. Scale bars: 500 μm.

Figure S3 (related to Figure 1). Generation of ganglionic eminence organoids with mature interneurons.

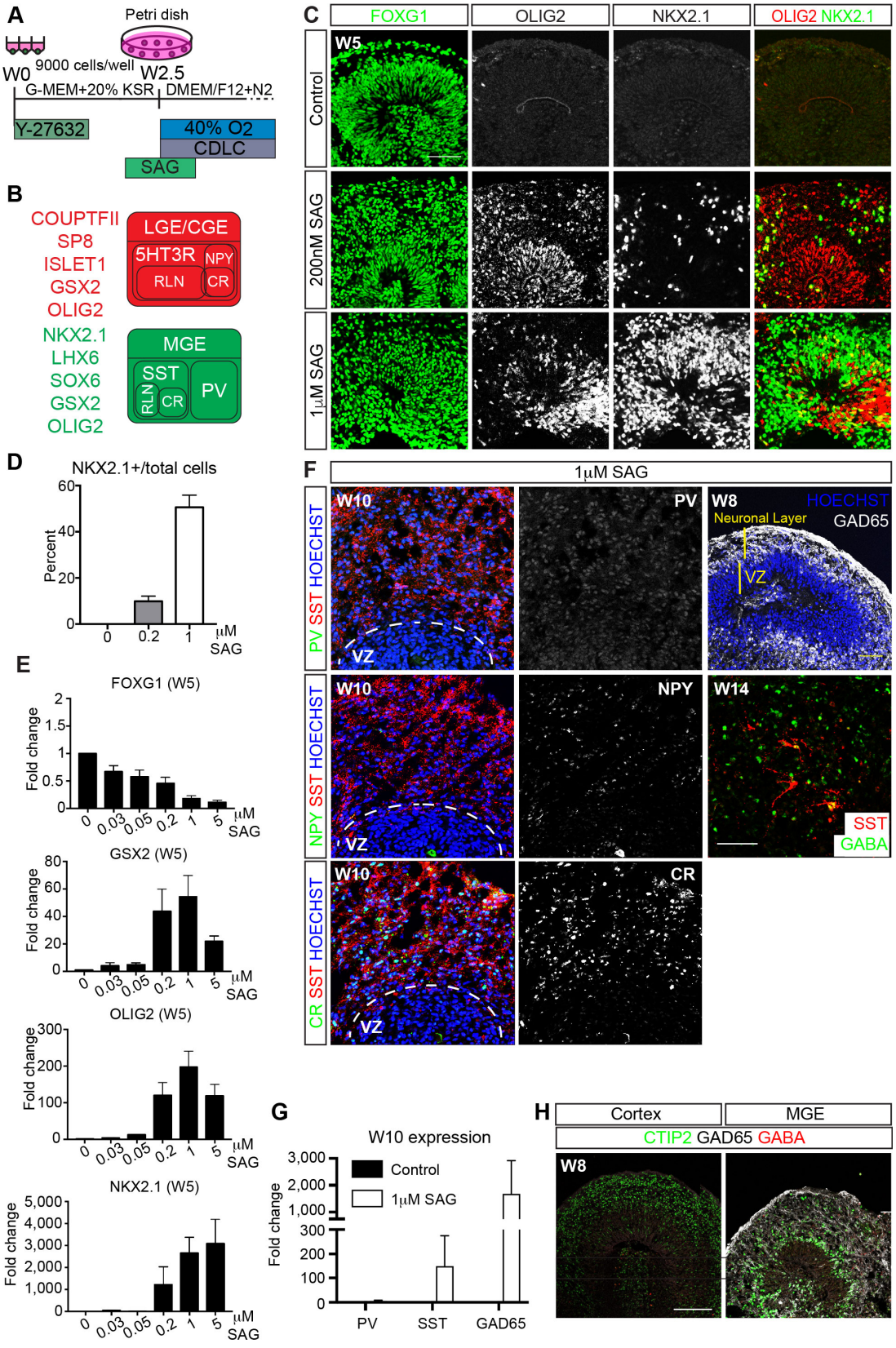

(**A**) Modified cerebral organoid protocol (see Fig. S1A) with addition of SAG from day 15-21 to create LGE/MGE/CGE organoids. (**B**) Schematic of progenitor and interneuronal markers for LGE, MGE, and CGE. (**C**) W5-organoids immunostained for regional markers, FOXG1, OLIG2, and NKX2.1. (**D**) Average number of $NKX2.1^+$ cells per W5-organoid. n=3. (**E**) RT-qPCR demonstrating upregulation of regional markers in a SAG-dose dependent manner. Fold change relative to control organoids without SAG addition. n=4-10 per condition. Data are represented as mean ± SEM. (**F**) MGE/CGE organoids at W10 immunostained for cortical interneuronal markers: SOMATOSTATIN (SST), PARVALBUMIN (PV), NEUROPEPTIDE Y (NPY), and CALRETININ (CR). W8-GE organoids showing laminar structure, with VZ progenitor region and neuronal layer positive for GAD65. W14 MGE organoid immunostained for SST and mature interneuronal marker GABA. (**G**) RT-qPCR for interneuronal markers. Fold change relative to cortical organoids without SAG addition. n=3. (H) W8 cortical and ganglionic eminence organoids immunostained for CTIP2, GAD65, and GABA. Note CTIP2 expression in cortical organoids is exclusive of striatal markers. Data in panels D, E, and G are represented as mean ± SEM. Scale bars: C, F 50 μm.

Figure S4 (related to Figure 3). STAT3 activation by addition of LIF in cerebral organoids.

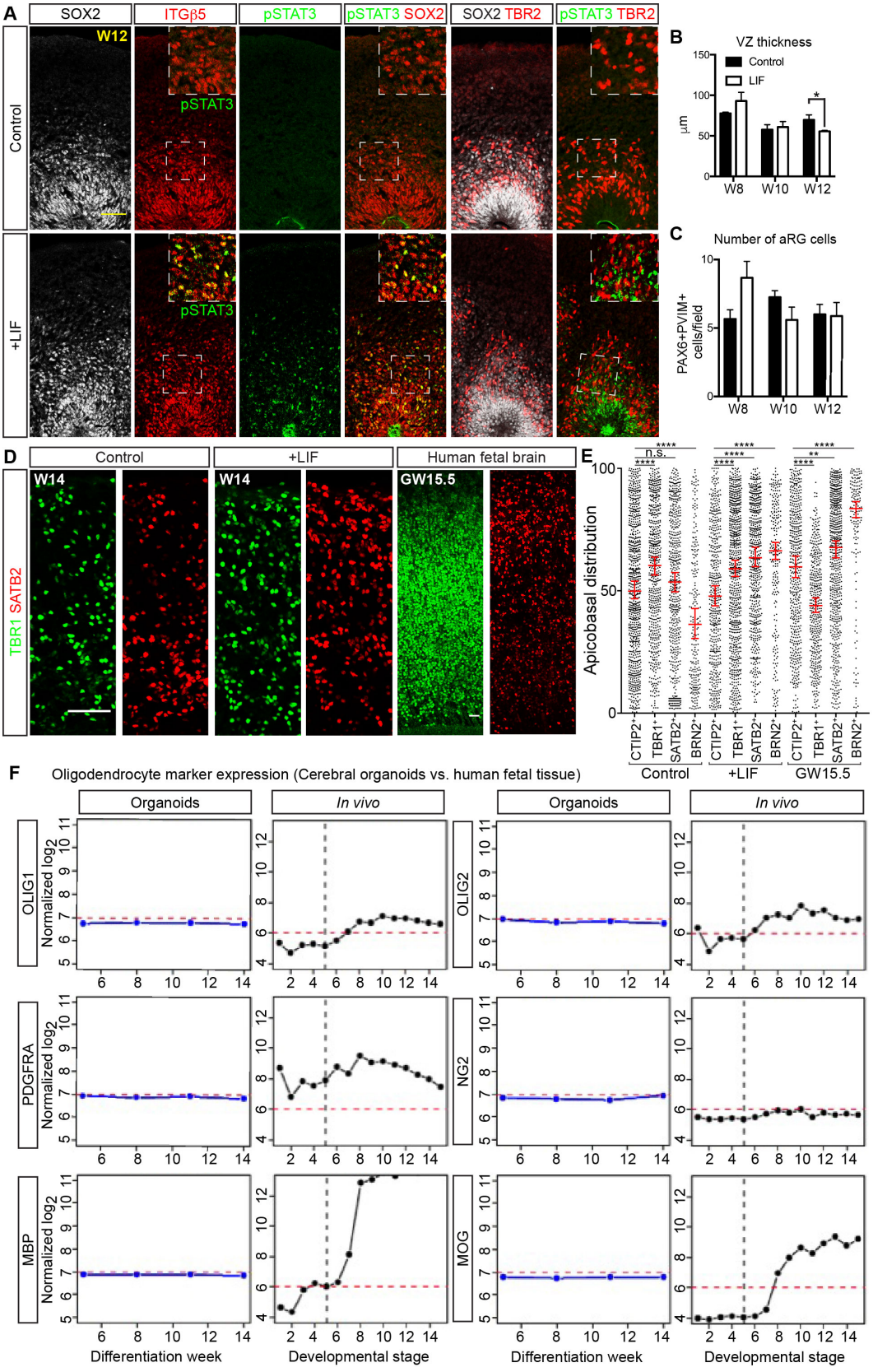

(**A**) Cerebral organoids immunostained for progenitor (SOX2), RG cell (ITGβ5), IP (TBR2), and STAT3 activated cell (pSTAT3) markers. (**B**) Continued from Fig. 3D, size of ventricular zone (VZ) in μm. W8 n=3, W10 Control n=3 LIF n=5, W12 n=7. Data are represented as mean ± SEM. (**C**) Continued from Fig. 3D, number of aRG. aRG counted as number of $PAX6^+$ and $pVIM^+$ cells dividing at the apical VZ surface. W8 n=3, W10 Control n=4 LIF n=5, W12 Control n=7 LIF n=8. Data are represented as mean ± SEM. (**D**) Cerebral organoids immunostained for lower layer neuronal (TBR1) and upper layer neuronal (SATB2) markers. (**E**) Continued from Fig 3F. Relative position of $CTIP2^+$, $TBR1^+$, $SATB2^+$ and $BRN2^+$ neurons. Values represent median ± 95%CI. Total number of neurons counted from 3 independent experiments, Control: $CTIP2^+$ n=756, $TBR1^+$ n=572, $SATB2^+$ n=538, $BRN2^+$ n=239; LIF: $CTIP2^+$ n=479, $TBR1^+$ n=716, $SATB2^+$ n=556, $BRN2^+$ n=230; GW15.5: $CTIP2^+$ n=492, $TBR1^+$ n=409, $SATB2^+$ n=622, $BRN2^+$ n=161. n.s. no significance, $^{**}p < 0.01$, $^{***}p<0.001$, $^{****}p < 0.0001$, Statistical analysis compares indicated neuronal marker to the $CTIP2^+$ group, Kruskal-Wallis test with Dunn's Correction. (**F**) Oligodendrocyte markers OLIG1, OLIG2, PDGFRA, NG2, MBP, and MOG are expressed below threshold in cerebral organoids compared to in vivo expression profiles by microarray analyses. In vivo developmental stages outlined in Fig. 2C. Scale bars: A, D 50 μm.

Figure S5 (related to Figure 3). Astrocyte production in cortical organoids compared to human neonatal brain tissues.

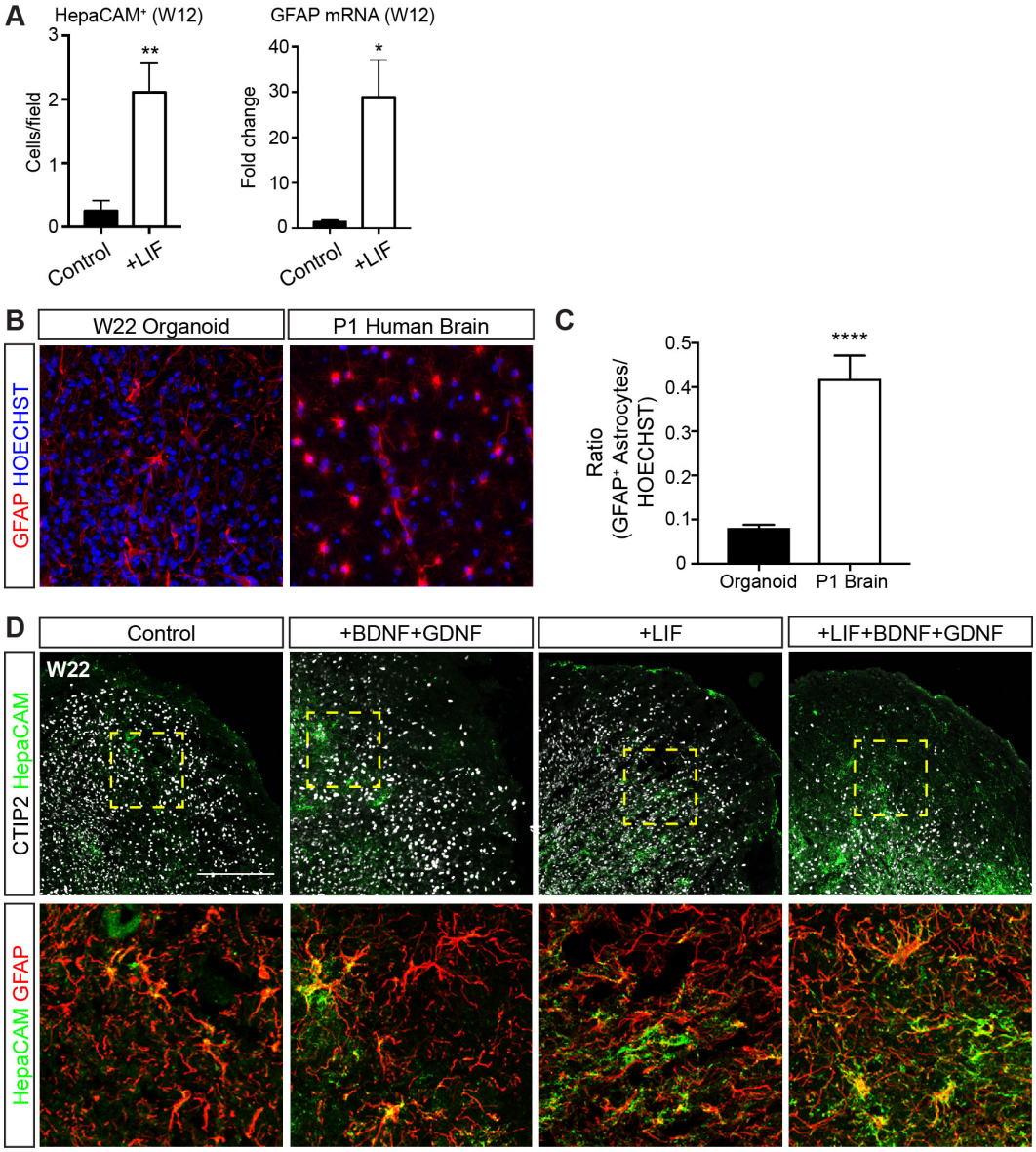

(**A**) Continued from Fig. 3E. RT-qPCR for GFAP expression. Fold change relative to organoids without LIF treatment (n=4) are plotted. Number of HepaCAM$^+$ star-like astrocytes per field. n=8 control, n=9 LIF treated organoids. Data are represented as mean ± SEM. (**B-C**) Comparison of GFAP$^+$ astrocyte densities of W22 cortical organoids to post-mortem neonatal (P1) human brain tissue. Chart indicates mean frequency of GFAP expression relative to total number of cells. Data are represented as mean ± SEM. (**D**) Combinatorial actions of growth factors (BDNF/GDNF) and LIF in promoting astrocyte formation (GFAP$^+$ astrocytes) and maturation (HepaCAM$^+$ astrocytes). Scale bar: D 200 µm.

Figure S6 (related to Figure 4). Efficient infection with calcium indicator AAV1-SYN::GCaMP6f and spontaneous ensemble neuronal activities in cerebral organoids.

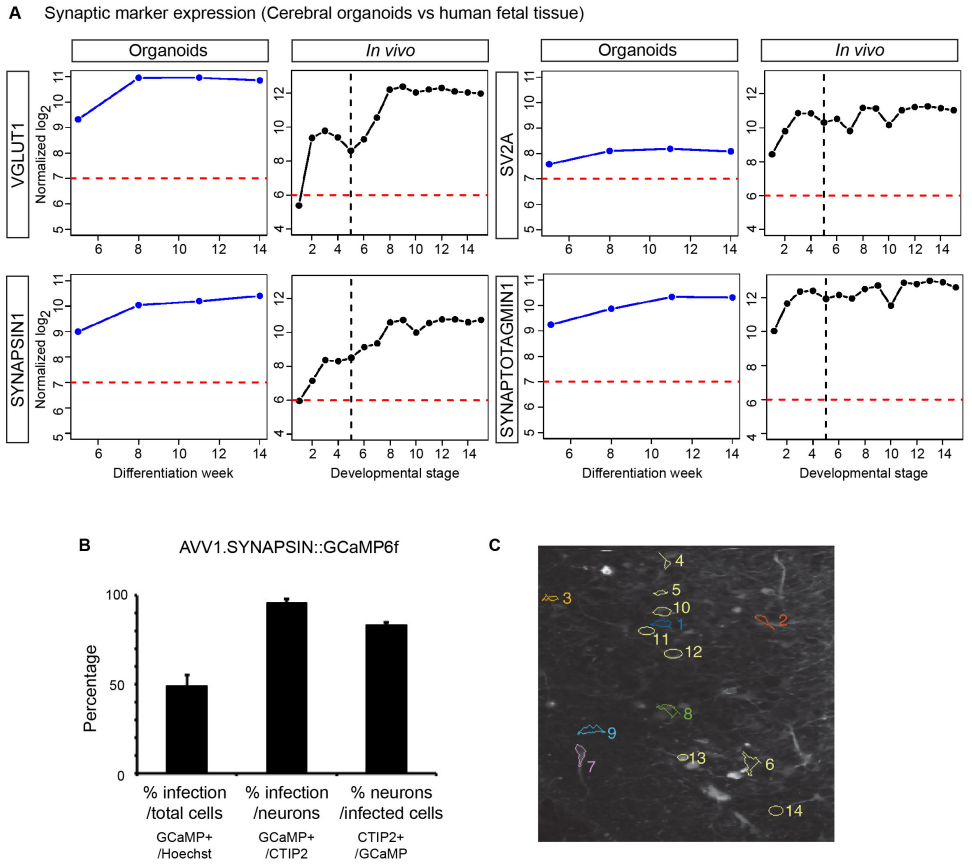

(**A**) Synaptic markers VGLUT1, SV2A, SYNAPSIN1, and SYNAPTOTAGMIN1 were expressed above threshold in cerebral organoids by microarray analyses. In vivo expression profiles also showed high expressions of these synaptic markers. In vivo developmental stages outlined in Fig. 2C. (**B**) Infection efficiency of adeno-associated virus AVV1-SYNAPSIN::GCaMP6f. Percentage of total cells ($GCaMP^+$/HOECHST), percentage of neurons infected ($GCaMP^+$/$CTIP2^+$), and percentage of neurons out of infected cells ($CTIP2^+$/$GCaMP^+$) n=3. Data are represented as mean ± SEM. (**C**) Mean field of view of one organoid during two-photon imaging and detected neuronal segments exhibiting fast calcium transients. These 14 segmented neurons were used for the analyses in Fig. 4H-J. Color-coded segments correspond to example traces in Fig. 4H. See also Movie S1.

Figure S7 (related to Figure 5). Expression profiles of ZIKV susceptibility receptors and impact of ZIKV on cultured spinal cord and cortical progenitors.

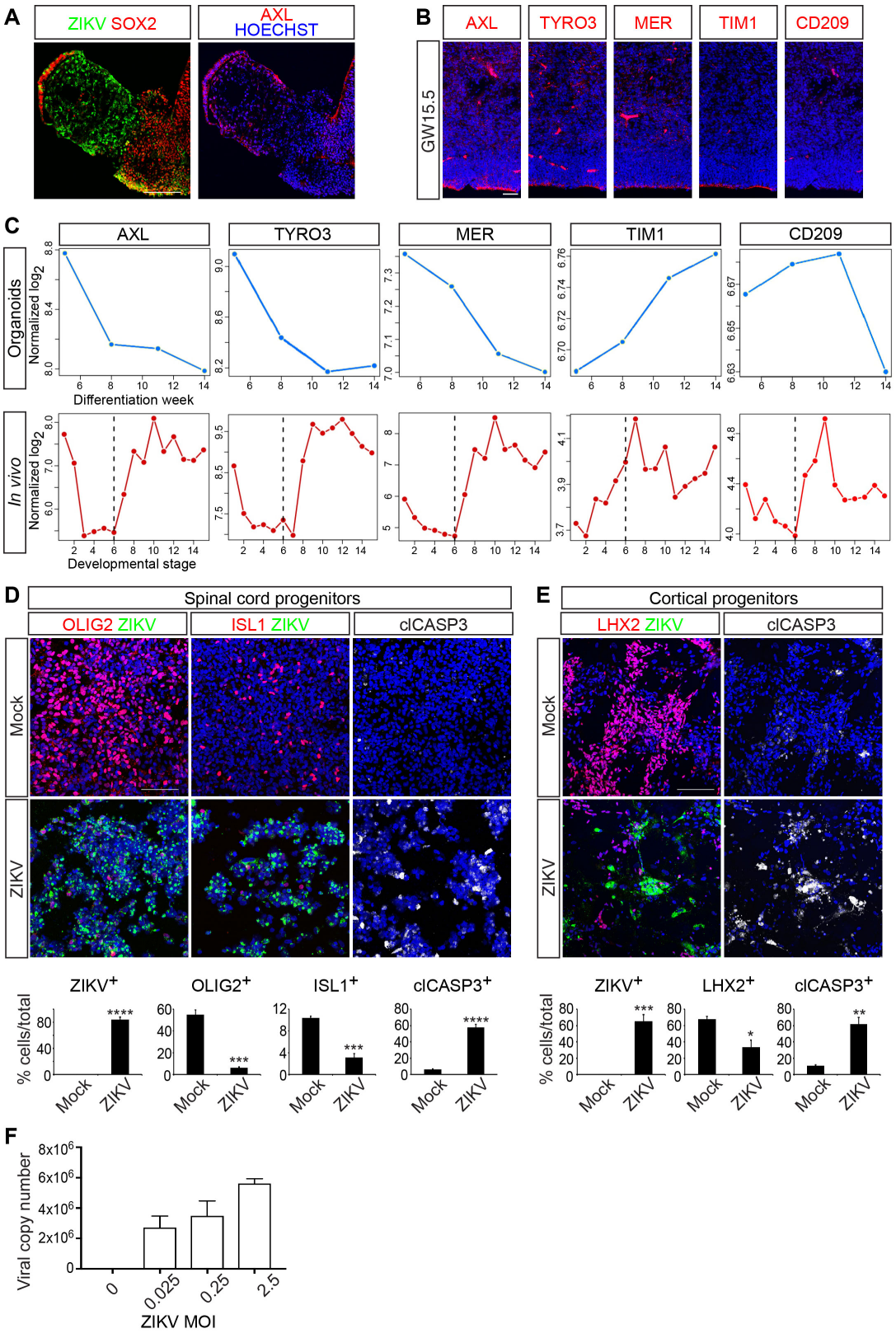

(**A**) Continued from Fig. 5B. The choroid plexus-like structure highly positive for ZIKV and AXL, but negative for SOX2. (**B**) VZ/SVZ regions of GW15.5 human fetal brain stained with HOECHST and antibodies against the ZIKV candidate receptors AXL, TYRO3, MER, TIM1, and CD209. (**C**) Expression of ZIKV candidate receptors in different weeks of cerebral organoids and in vivo developmental stages by microarray analyses. In vivo developmental stages are outlined in Fig. 2C. (**D**) W3-spinal cord progenitors infected with ZIKV. Cells were stained with HOECHST (blue) and antibodies recognizing ZIKV, motor neuron progenitors (OLIG2), differentiated motor neurons (ISL1), and the cell death marker clCASP3. The percentages of the total cell population expressing ZIKV envelope, OLIG2, ISL1, and clCASP3 with and without ZIKV infection are displayed. n=3 experiments. (**E**) Cortical progenitors infected with ZIKV. W6-organoids were dissociated and plated in an adherent culture for infection. Cells immunostained for ZIKV, telencephalic marker (LHX2), and cell death (clCASP3). The percentages of the total cell population expressing ZIKA envelope, LHX2, and clCASP3 are displayed. n=3 experiments. (**F**) RT-qPCR results of viral copy numbers in W3 organoids collected 3 days post infection with various MOI of ZIKV. Data in panels D-F are represented as mean ± SEM. All scale bars: 100 μm.

Figure S8 (related to Figure 6). Transcriptomic analyses of cerebral organoids infected with ZIKV by RNA sequencing.

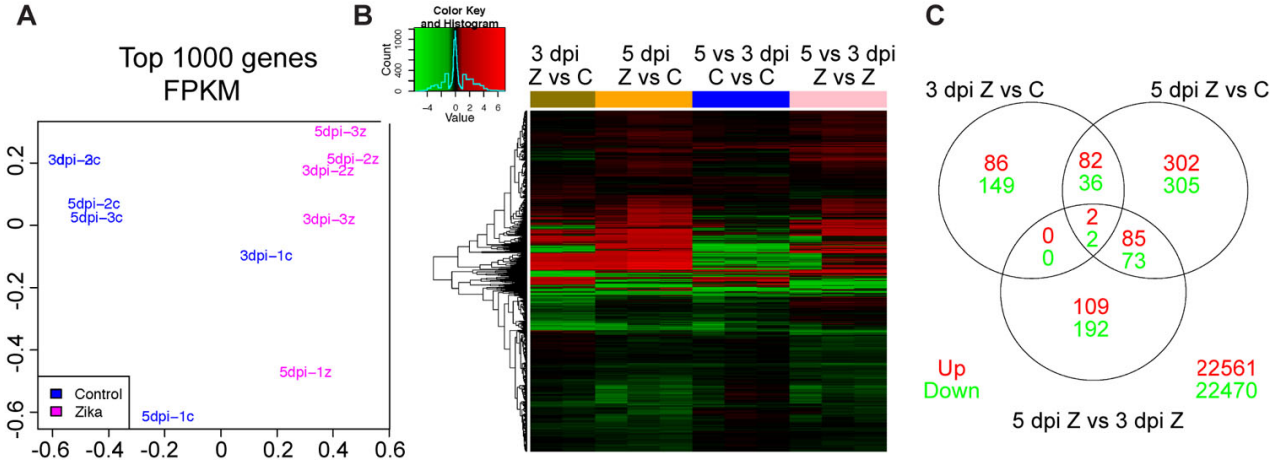

W8 organoids were infected with ZIKV and analyzed at 3 and 5 days post infection (dpi). Each condition had n=3 independent replicates. One outlier (a 3-day control) was removed from the analysis. (**A**) Multiple-dimensional scaling using Fragments Per Kilobase of transcript per Million mapped reads (FPKM) values showed that expression changes associated with ZIKV infection drive most of the observed variability in gene expression. (**B**) Heatmap and clustering of differentially expressed at $p < 0.005$. Green color in the heatmap indicates downregulated, and red upregulated transcripts, Z=ZIKV and C=control. (**C**) Venn diagram of the transcripts dysregulated by ZIKV at 3 and 5 days (top 2 circles) and ZIKV at 5 dpi vs. ZIKV at 3 dpi (bottom circle). Upregulated and downregulated transcripts are in red and green, respectively.

Figure S9 (related to Figure 7). Comparison of the efficacy of different agents in blocking ZIKV infection of cerebral organoids.

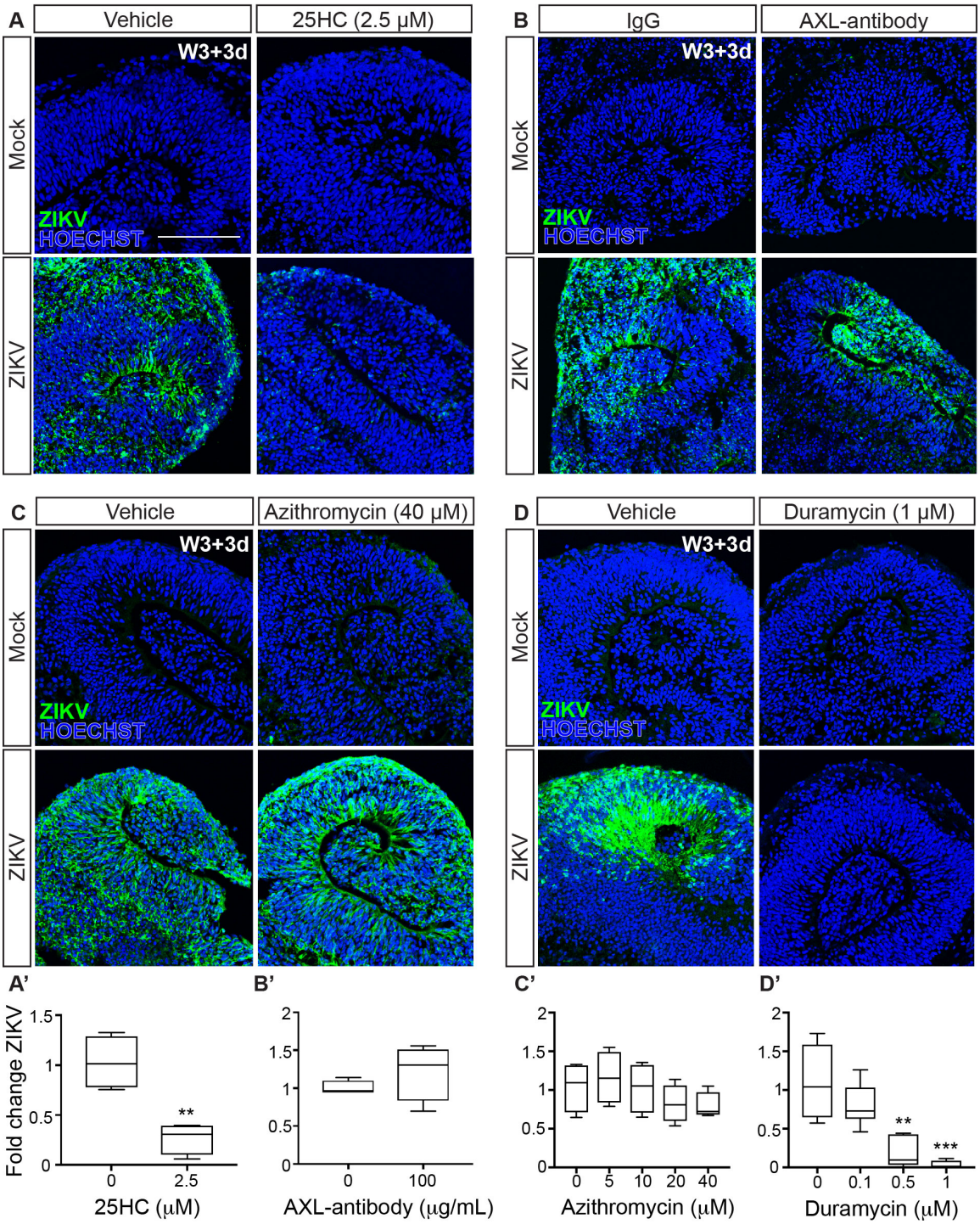

Cerebral organoids immunostained for ZIKV 3dpi in the absence or presence of (**A**) 25HC, (**B**) AXL-antibody, (**C**) Azithromycin, and (**D**) Duramycin. Scale bar: 100 µm. (**A'-D'**) qPCR analysis of ZIKV expression. Plots represent expression levels normalized to ZIKV-vehicle average. Data are represented as mean ± SEM. (**A'**) 25HC n=4, (**B'**) AXL-antibody n=4, (**C'**) Azithromycin n=4, and (**D'**) Duramycin n=6. See also Table S5 for statistical analysis details.

SUPPLEMENTAL TABLES

Table S1 (related to Figure 2). Summary of High-Confidence Modules in Human Fetal Cortex and Cerebral Organoid

Module Number	Module Color	In vivo Pzscore	Organoid Pzscore	Select Hub Genes
4	Magenta	17.0	29	BUB1, BUB1B, KIF20A
3	Red	21.0	23	ACTL6A, HIST1H3H, HIST1H2BM, BUB3, CDK4, CNOT1, SRSF1
8	Salmon	14.0	18	GRIN1, GRID1, SLC1A1, CAMK2β, VAMP2, SYT3/5
14	Purple	10.0	18	SEMA4G, SEMA6C, CRMP1, SRGAP1, DCX
27	Cyan	4.1	16	NRXN1, PCLO, ANK2/3, MAPT, MYO5A, KIF3B/C, DOCK9
5	Pink	15.0	16	HES1, NOTCH2, FGFR3, RFX4
11	Lightgreen	12.0	14	GABRA2/5, GABRG2/3, GLRB, SNAP25, SYT1, SV2A
2	Green	28.0	12	GRIA4, GRIK4, GRIN3A, SHANK2, RIMS1, SV2B, CACNA1I
15	Grey60	9.8	5.7	THOC1, RBM39, PNN, MRE11A, POLA1, POLE, CNTRL
20	Paleturquoise	5.8	5.2	CACNA2D2, CHRFAM7A, SLC24A2
18	Darkred	5.9	4.8	DKK1, BOK, RNF152
6	Turquoise	15.0	4.4	KLHL9, CRNKL1, CREB1, HDAC2, SENP1
19	Lightcyan	6.3	3.1	LAMA2/4, COL3A1, COL1A1/2, BMP4, SMAD6
23	Darkturquoise	5.0	1.5	NAPA, SORT1, AP2M1, ARF1, MAPK3
7	Midnightblue	14.0	1.1	MLL1/4/5, CHD2/3, SMARCA4, CREBBP, FOXG1
1	Yellow	31.0	0.92	CAMK2A, GRIK1, GFAP, AQP4, CX3CL1
9	Tan	13.0	0.91	STAT6, TGFBR2/3, CXCL12, CALCRL, TGM2
26	Darkolivegreen	4.5	0.4	COPA, COPE, COPG, VPS11, VAC14, SNAP29
16	Skyblue3	8.8	0.38	SLC17A7, PCDH9, CNTNAP5, ARHGAP44, MGLL
25	Greenyellow	4.7	-0.083	RBFOX1, LUC7L3, CAPRIN2
12	Orange	11.0	-0.5	CX3CR1, TYROBP, LAPTM5, CSF1R
10	Black	12.0	-2.4	BTN3A3, CFB, CTSS, DHX58, HERC5

Module Number	Module Color	Biological Processes Associated with Module
4	Magenta	Mitosis and cell cycle regulation of neural progenitors
3	Red	Mitosis, RNA processing and RNA splicing
8	Salmon	Glutamatergic synaptic transmission, axon and dendrite development
14	Purple	Axon guidance and GTPase activity
27	Cyan	Synapse assembly and vesicle transport by actin/microtubule motors
5	Pink	Neural progenitor proliferation and gliogenesis
11	Lightgreen	GABAergic synaptic transmission and synaptic vesicle exocytosis
2	Green	Glutamatergic synaptic transmission, axon and dendrite development
15	Grey60	RNA splicing, DNA repair and cell cycle
20	Paleturquoise	Synaptic transmission
18	Darkred	Programmed Cell Death
6	Turquoise	Ubiquitin proteolysis, RNA processing and splicing
19	Lightcyan	Extracellular matrix and basement membrane, blood vessel develop.
23	Darkturquoise	Intracellular protein transport, vesicle and endosome trafficking
7	Midnightblue	Histone modification and chromatin remodeling
1	Yellow	Synaptic transmission, gliogenesis and neuron microglia interaction
9	Tan	Reg. of cell death, gliogenesis, immune and inflammatory processes
26	Darkolivegreen	Intracellular protein transport, vesicle and endosome trafficking
16	Skyblue3	Neuronal, synaptic with parietal areal identity
25	Greenyellow	RNA binding
12	Orange	Immune response, neuron-microglia interaction
10	Black	Immune response

Module preservation Z scores are shown for developing human cortex and cerebral organoids (W5 vs W14). Modules not preserved in organoids are highlighted in pink and modules preserved in both in vivo and in vitro are highlighted in green. Some modules with few genes (<70) lacking clear GO enrichment are preserved in vivo (white, steelblue, saddlebrown, yellowgreen, and violet), but not shown here. For detailed explanation, see Stein et al., 2014.

Table S2 (related to Figure 6). Top 50 Upregulated Transcripts upon ZIKV infection at 3 and 5 dpi

Transcript	3 dpi ZIKV vs Control	Transcript	5 dpi ZIKV vs Control
SAMD9	4.753351054	OAS2	6.323266235
SAMD9L	4.554938175	OAS1	6.021227692
CCL5	4.359314	OAS3	5.940906319
OAS1	4.143859296	IFNB1	5.905361296
OAS3	4.111865889	SAMD9	5.789032826
IFIT3	4.04078647	CXCL11	5.692781558
MX1	4.032918155	CCL5	5.650141418
IFIT2	4.027343073	MX1	5.510042181
APOL6	3.893887571	IFIT3	5.255483595
IFIT1	3.751789987	SAMD9L	4.920016749
NLRC5	3.67156849	IFIT1	4.802510386
OAS2	3.670840265	IFIT2	4.788387276
CETP	3.628899582	ISG15	4.682414836
ISG15	3.591420312	APOL6	4.60053119
EPSTI1	3.51701378	IFI6	4.522604346
IFIH1	3.50916866	RSAD2	4.501210753
PSMB9	3.385254396	IFIH1	4.325888388
CXCL11	3.287714624	RTP4	4.164585412
RSAD2	3.248432975	EPSTI1	4.140104287
CMPK2	3.143771397	NLRC5	4.130342071
RTP4	3.10090871	CH25H	4.086323415
ETV7	3.093105384	CSAG1	4.072637577
DDX58	3.064415012	AMELX	4.0661765
DDX60L	3.058867118	HLA-F	4.0634779
IFI6	3.045716203	BATF2	4.002454516
PARP12	3.045020356	PSMB9	3.899302166
NRIR	3.017409598	EPHA1-AS1	3.859016281
CXCL1	2.976721457	SP100	3.819080243
HLA-F	2.959126403	CMPK2	3.792209462
SP110	2.911714523	NRIR	3.745833147
PLSCR1	2.838427277	PARP12	3.676653659
STAT1	2.804882248	APOL1	3.672189732
CH25H	2.799824636	ETV7	3.639138229
MX2	2.794462907	KCNJ15	3.633657828
DTX3L	2.777284737	HLA-DOB	3.579509657
IFNB1	2.755846069	DHX58	3.51738449
HERC6	2.7294792	IFI27	3.490603706
SLC15A3	2.70493507	STAT1	3.48421462
PARP9	2.65177229	PLSCR1	3.425689989
DHX58	2.605990884	GBP5	3.397782015
DDX60	2.602487057	IRF9	3.357768087
ZFAT-AS1	2.597852965	DDX60L	3.357203896
IRF9	2.59356195	MX2	3.356232774
HERC5	2.58338294	DDX60	3.343639004
SP100	2.578462728	DDX58	3.319701461
NMI	2.566705041	HERC6	3.316546043
KCNJ15	2.539346778	HERC5	3.315617755
HELZ2	2.535506379	RUFY4	3.311808007
LINC01498	2.533504566	IFITM1	3.257276443
C5orf56	2.528659148	PSMB8-AS1	3.227617874

Upregulated transcripts ($p < 0.005$) upon ZIKV infection. Gene expression changes are expressed as $\log_2$ (fold change). dpi, days post infection. Genes upregulated and related to immune response and function at both 3 and 5 dpi are highlighted in yellow and orange. Orange genes are further implicated in anti-viral activities.

Table S3 (related to Figure 6). Top 50 Downregulated Transcripts upon ZIKV infection at 3 and 5 dpi

Transcript	3 dpi Z vs Control	Transcript	5 dpi ZIKV vs Control
HMGCS2	-2.947360279	LINC00920	-3.137656504
LOC100996255	-2.92994189	BFSP2	-2.797856937
GBX1	-2.701140164	SLC22A6	-2.764903145
LOC101929371	-2.64137911	HEPACAM	-2.697454936
CLCNKB	-2.56514082	LINC01212	-2.586317051
HOTAIR	-2.533631619	MYF6	-2.561210489
LOC100652999	-2.507660192	PAX8-AS1	-2.55927715
HOXC10	-2.457727936	PGR	-2.503568569
SLC28A3	-2.446843068	HABP2	-2.491847251
LINC01160	-2.439193152	NAT8B	-2.42594284
ALDH1L1-AS1	-2.434942587	IQCJ	-2.415030183
MZB1	-2.305799317	SNORA35	-2.351284677
PRRX2	-2.289480201	LOC102724050	-2.241734813
SLC22A6	-2.284554125	DKFZP434L187	-2.183969025
MIR23A	-2.283722461	MIR1298	-2.124655733
ZNF541	-2.283083756	PRKACG	-2.07027174
PCDHB1	-2.282399168	HOXC10	-2.052923768
PHYHD1	-2.261108299	RFX8	-2.006558464
MIR219A2	-2.255361976	C2orf91	-1.94123325
LINGO4	-2.255361976	LINC00934	-1.93686752
CFTR	-2.050334748	LINC00605	-1.922749767
EMR2	-2.040911245	LOC100507537	-1.877579774
HABP2	-2.023870876	HIST1H2BH	-1.868946039
SNORD115-10	-2.016944151	DUSP27	-1.69615308
SLC39A12	-1.970748618	HDC	-1.672321696
LOC102546229	-1.912540937	SNORD77	-1.584689192
LOC100288814	-1.8858107	CFAP44-AS1	-1.498273916
SLC38A11	-1.862570399	HIST1H3E	-1.466387422
SLC17A8	-1.847430172	GPR151	-1.336329005
NRN1L	-1.808372176	SLC17A8	-1.332902614
PRND	-1.79930009	PRND	-1.327989445
TTLL6	-1.785026198	TTLL6	-1.298819177
MIR4677	-1.785026198	ALDH1A3	-1.294508635
HRH4	-1.681812367	GUCY2F	-1.249219419
ATP13A4-AS1	-1.677103063	CFTR	-1.223088217
PEG3	-1.671028719	LOC100652999	-1.216625019
NPPB	-1.644969496	SLC39A12	-1.167204083
IGFL3	-1.571331344	BLNK	-1.147632076
IL5RA	-1.568894753	RXFP3	-1.048754355
INTS4P2	-1.535470259	NMU	-1.032510439
GPR1	-1.516290525	GPR1	-0.985267905
LOC253573	-1.514197676	C1orf168	-0.959538796
HDC	-1.482224243	NDNF	-0.926174556
WFIKKN2	-1.457536479	PLS3	-0.913887422
C1orf110	-1.428698074	NKAPP1	-0.911018957
C2orf91	-1.428581203	LINC01470	-0.901738232
GUCY2F	-1.387882336	WNT8B	-0.880326435
HOXC-AS2	-2.947360279	RSPO1	-0.876116464
MEIS1-AS3	-2.92994189	GPC3	-0.83652628
PLA1A	-2.701140164	BTBD11	-0.814469345

Downregulated transcripts ($p < 0.005$) upon ZIKV infection. Gene expression changes are expressed as $\log_2$ (fold change). dpi, days post infection.

Table S4 (related to Figure 4). Electrophysiological properties of neurons in cortical organoids and *in vivo* fetal tissue

Table S4: Cortical organoid neurons electrophysiology Figure 4D							
	APs?	Average	SEM	n	Statistical test*	p-value	Significance
Membrane Potential (mV)	APs No APs	-60.2 -57.1	2.2 3.4	12 cells 12 cells	Unpaired	0.4479	n.s.
Membrane Resistance (ΩG)	APs No APs	2.94 2.81	0.58 0.44	12 cells 12 cells	Mann-Whitney	0.8603	n.s.
Capacitance (pF)	APs No APs	14.4 8.3	3.6 1.0	12 cells 12 cells	Mann-Whitney	0.2189	n.s.
Current at -25mV (peak Na+ current pA)	APs No APs	-1.01 0.21	0.32 0.04	12 cells 12 cells	Mann-Whitney	<0.0001	****
Current at 45mV (peak K+ current pA)	APs No APs	1.32 0.74	0.21 0.14	12 cells 12 cells	Mann-Whitney	0.0029	**

Midgestational neurons (GW16-22) in CP of human fetal cortex (Moore et al. 2009)			
	Average	SEM	n
Membrane Potential (mV)	-49.8	1.3	161 cells
Membrane Resistance (ΩG)	3.05	0.18	161 cells
Capacitance (pF)	15.6	0.88	161 cells
Current at -25mV (peak Na+ current pA)	-0.42	0.05	161 cells
Current at 45mV (peak K+ current pA)	0.38	0.03	161 cells

APs = action potentials. Statistical tests: Two-tailed unpaired t-test "unpaired", Two-tailed unpaired t-test with Welch's correction "Welch", and Mann-Whitney U Test "Mann-Whitney". n.s. = not significant p-value >0.05.

Table S5 (related to Figures 7 and S9). Statistics and p-values for Figures 7 and S9

		Average ± SEM	n	Statistical test*	p-value	Significance
Figure 7A: 25HC 7 dpi						
RT-qPCR	0 µM + ZIKV 2.5 µM + ZIKV	1.022 ± 0.09476 0.2657 ± 0.0732	6 replicates	Unpaired	<0.0001	****
Flavivirus %	0 µM + ZIKV 2.5 µM + ZIKV	62.41 ± 2.21 17.46 ± 2.12	6 images 6 images	Unpaired	<0.0001	****
clCASP3 %	0 µM Mock 2.5 µM Mock	7.38 ± 1.00 13.48 ± 1.01	6 images 6 images	Unpaired	0.0016	**
	0 µM + ZIKV 2.5 µM + ZIKV	24.34 ± 1.77 23.12 ± 1.94	6 images 6 images	Unpaired	0.6506	n.s.
Figure 7B: R428 7 dpi						
RT-qPCR	0 nM + ZIKV 30 nM + ZIKV 300 nM + ZIKV 1 µM + ZIKV	1.012 ± 0.07623 0.8858 ± 0.1075 0.9392 ± 0.07019 0.5974 ± 0.1405	5 replicates	 Unpaired Unpaired Unpaired	 0.3679 0.5049 0.0321	 n.s. n.s. *
Flavivirus %	0 nM + ZIKV 1 µM + ZIKV	35.21 ± 6.35 19.81 ± 4.10	7 images 7 images	Unpaired	0.0642	n.s.
clCASP3 %	0 nM Mock 1 µM Mock	6.59 ± 1.79 7.18 ± 0.95	4 images 5 images	Unpaired	0.7975	n.s.
	0 nM + ZIKV 1 µM + ZIKV	21.03 ± 3.19 11.07 ± 0.97	7 images 7 images	Welch	0.0200	*
Figure 7C: Duramycin 7 dpi						
RT-qPCR	0 µM + ZIKV 0.1 µM + ZIKV 0.5 µM + ZIKV 1 µM + ZIKV	1.014 ± 0.1163 0.9704 ± 0.05768 0.1456 ± 0.04917 0.1859 ± 0.09298	3 replicates	 Unpaired Unpaired Unpaired	 0.7510 0.0023 0.0051	 n.s. ** **
Flavivirus %	0 µM + ZIKV 1 µM + ZIKV	51.51 ± 6.10 0.96 ± 0.52	7 images 8 images	Welch	0.0002	***
clCASP3 %	0 µM Mock 1 µM Mock	7.47 ± 1.83 6.29 ± 1.99	2 images 7 images	Welch	0.6854	n.s.
	0 µM + ZIKV 1 µM + ZIKV	27.06 ± 4.95 5.11 ± 0.51	8 images 8 images	Welch	0.0030	**
Figure 7D: Ivermectin 7 dpi						
RT-qPCR	0 nM + ZIKV 500 nM + ZIKV	1.013 ± 0.101 0.04256 ± 0.02448	4 replicates	Unpaired	<0.0001	****
Flavivirus %	0 nM + ZIKV 500 nM + ZIKV	85.18 ± 4.12 2.22 ± 0.64	8 images 8 images	Welch	<0.0001	****
clCASP3 %	0 nM Mock 500 nM Mock	4.98 ± 0.69 8.66 ± 1.31	9 images 8 images	Unpaired	0.0216	*
	0 nM + ZIKV 500 nM + ZIKV	16.80 ± 2.21 8.88 ± 0.96	8 images 8 images	Welch	0.0086	**
Figure S7 A': 25HC 3 dpi						
RT-qPCR	0 µM + ZIKV 2.5 µM + ZIKV	1.027 ± 0.1359 0.2678 ± 0.07895	4 replicates	Unpaired	0.0029	**
Figure S7 B': AXL-antibody 3 dpi						
RT-qPCR	0 µg/mL + ZIKV 100 µg/mL+ZIKV	1.003 ± 0.04615 1.216 ± 0.1843	4 replicates	Unpaired	0.3045	n.s.
Figure S7 C': Azithromycin 3 dpi						
RT-qPCR	0 µM + ZIKV 5 µM + ZIKV 10 µM + ZIKV 20 µM + ZIKV 40 µM + ZIKV	1.041 ± 0.161 1.161 ± 0.1685 1.028 ± 0.1602 0.8231 ± 0.1228 0.792 ± 0.08743	4 replicates	 Unpaired Unpaired Unpaired Unpaired	 0.6261 0.9552 0.3234 0.2231	 n.s. n.s. n.s. n.s.
Figure S7 D' Duramycin 3 dpi						
RT-qPCR	0 µM + ZIKV 0.1 µM + ZIKV 0.5 µM + ZIKV 1 µM + ZIKV	1.1 ± 0.2063 0.8027 ± 0.1123 0.1842 ± 0.0798 0.03577 ± 0.01984	6 replicates	 Unpaired Unpaired Unpaired	 0.2350 0.0020 0.0004	 n.s. ** ***

dpi= days post infection with Zika virus (ZIKV). Statistical tests: Two-tailed unpaired t-test "unpaired", Two-tailed unpaired t-test with Welch's correction "Welch", and Mann-Whitney U Test "Mann-Whitney". n.s. = not significant p-value >0.05.

Table S6. Key Resources

REAGENT or RESOURCE	SOURCE	IDENTIFIER
Antibodies		
See Table S7 for list of Antibodies	N/A	N/A
Biological Samples		
Human fetal brain GW 14-17	Novogenix Laboratories	N/A
Human fetal tissue GW 4	University of Tübingen	N/A
Chemicals, Peptides, and Recombinant Proteins		
ESGRO Mouse Recombinant Leukemia Inhibitory Factor (mLIF)	EMD Millipore	ESG1106
InSolution Smoothened Agonist (SAG)	EMD Millipore	566661
25-Hydroxycholesterol (25HC)	Sigma-Aldrich	H1015
Duramycin	Molecular Targeting Technologies, Inc.	D-1005
Ivermectin	Sigma-Aldrich	I8898
Azithromycin	Sigma-Aldrich	PZ0007
R428	MedChem Express	HY-15150
Human AXL-antibody	R&D Systems	AF154
Normal Goat IgG Control	R&D Systems	AB-108-C
Critical Commercial Assays		
miRNeasy Mini Kit	Qiagen	217044
RNeasy Mini Kit	Qiagen	74106
SuperScript IV First-Strand Synthesis System	Thermo Fisher Scientific	18091200
Deposited Data		
Microarray data	Gene Expression Omnibus (NCBI)	GSE97872
RNA-seq data	Gene Expression Omnibus (NCBI)	GSE97919
Experimental Models: Cell Lines		
H9 human embryonic stem cells	WiCell Research Institute (Thomson et al., 1998)	NIH 0062
UCLA1 human embryonic stem cells	UCLA Stem Cell Core at Broad Stem Cell Center (Diaz Perez et al., 2012)	NIH 0058
hiPS2 human induced pluripotent stem cells	UCLA Stem Cell Core at Broad Stem Cell Center (Lowry et al., 2008)	N/A
XFiPS Xeno-free human induced pluripotent stem cells	UCLA Stem Cell Core at Broad Stem Cell Center (Karumbayaram et al., 2012)	N/A
Aedes albopictus: C6/36 clone	ATCC CRL-1660	N/A
Experimental Models: Organisms/Strains		
Zika virus	Center for Disease Control and Prevention of United States (CDC)	Strain PRVABC59
AAV1.Syn.GCaM6f.WPRE.SV40	University of Pennsylvania Vector CORE	AV-1-PV2822

Recombinant DNA		
pLenti-Synapsin-hChR2(H134R)-EYFP-WPRE	Addgene	20945
Software and Algorithms		
Adobe Photoshop CS5, CS6	Adobe Systems Inc.	https://www.adobe.com
Image J	National Institutes of Health (Schneider et al., 2012)	https://imagej.nih.gov/ij/
GraphPad InStat	GraphPad Software	www.graphpad.com/scientific-software/instat/
GraphPad Prism 7	GraphPad Software	www.graphpad.com/scientific-software/prism/
CoNTExT	(Stein et al., 2014)	https://context.semel.ucla.edu
STAR	(Dobin et al., 2013)	https://code.google.com/archive/p/rna-star/
Limma-Voom	(Law et al., 2014)	www.bioconductor.org
EdgeR	(Robinson et al., 2010)	https://bioconductor.org
HTSeq		www.huber.embl.de/users/anders/HTSeq/doc/overview.html
Metascape		http://metascape.org
Other		
Statistical tests and p-values: See Table S4 and S5	This Study	N/A

Table S7. Primary Antibody List

Name	Species	Dilution	Vendor	Catalog #	Identifier
APKC (PKC zeta)	Rabbit	1:100	Santa Cruz Biotech	sc-216	RRID:AB_2300359
AQP1	Rabbit	1:500	EMD Millipore	ab2219	RRID:AB_1163380
AXL	Rabbit	1:100	Cell Signaling Tech	8661S	RRID:AB_11217435
BRN2 (POU3F2)	Goat	1:4000	Santa Cruz Biotech	sc-6029	RRID:AB_2167385
CALRETININ	Rabbit	1:2000	EMD Millipore	AB5054	RRID:AB_2068506
CAMKII alpha	Mouse	1:200	EMD Millipore	MAB3119	n/a
CASP-3 (activated)	Rabbit	1:500	Cell Signaling Tech	9661S	RRID:AB_2341188
CD209	Mouse	1:50	BioLegend	330103	RRID:AB_1134057
COUP-TF1 (NR2F1)	Mouse	1:1000	Perseus Proteomics	PP-H8132	RRID:AB_2155494
CTIP2 (BCL11B)	Rat	1:1000	Abcam	ab18465	RRID:AB_2064130
CUX1 (CDP) (B-10)	Mouse	1:100	Santa Cruz Biotech	sc-514008	RRID:AB_2715519
FLAVIVIRUS	Mouse	1:1000	EMD Millipore	MAB10216	RRID:AB_827205
FOXG1	Rabbit	1:1000	Abcam	ab18259	RRID:AB_732415
GABA	Rabbit	1:10000	Sigma-Aldrich	A2052	RRID:AB_477652
GAD65	Mouse	1:200	BD Biosciences	559931	RRID:AB_397380
GFAP	Rabbit	1:500	Abcam	ab7260-50	RRID:AB_305808
GFP	Sheep	1:800	ABD Serotec	4745-1051	RRID:AB_619712
GFP	Chicken	1:1000	Aves Lab Inc	GFP-1020	RRID:AB_10000240
GFP	Rabbit	1:4000	Invitrogen	A6455	RRID:AB_221570
HepaCAM	Mouse	1:500	R&D Systems	MAB4108	RRID:AB_2117687
HOPX	Rabbit	1:1000	Sigma-Aldrich	HPA030180	RRID:AB_10603770
ISL1	Goat	1:8000	R&D Systems	AF1837	RRID:AB_2126324
ITGβ5	Sheep	1:200	R&D Systems	AF3824	RRID:AB_1151977
LAMININ	Rabbit	1:1000	Abcam	ab30320	RRID:AB_775970
LHX2 (C-20)	Goat	1:1000	Santa Cruz Biotech	sc-19344	RRID:AB_2135660
MER (MERTK)	Mouse	1:50	R&D Systems	FAB8912P	RRID:AB_357214
N-CADHERIN	Mouse	1:1000	BD Biosciences	610920	RRID:AB_2077527
NESTIN	Mouse	1:1000	Neuromics	MO15012	RRID:AB_2148919
NEUROPEPTIDE Y	Rabbit	1:800	Abcam	ab10980	RRID:AB_297635
NKX2-1	Mouse	1:500	Novocastra	NCL-L-TTR-1	RRID:AB_564042
OLIG2 (252)	Guinea Pig	1:20000	Novitch lab (UCLA)	n/a	RRID:AB_2715520
OLIG2	Rabbit	1:5000	EMD Millipore	AB9610	RRID:AB_570666
PARVALBUMIN	Rabbit	1:5000	Abcam	AB11427-50	RRID:AB_298032
PAX6	Mouse	1:100	DSHB	Supernatant	RRID:AB_528427
PAX6	Rabbit	1:1000	MBL International	PD022	RRID:AB_1520876
pVIMENTIN	Mouse	1:500	MBL International	D076-3	RRID:AB_592963
pSTAT3 (Try705)	Rabbit	1:100	Cell Signaling Tech	9145P	RRID:AB_2491009
SATB2	Mouse	1:100	Abcam	ab51502	RRID:AB_882455
SOX2	Goat	1:100	Santa Cruz Biotech.	sc-17320	RRID:AB_2286684
SP8 (C18)	Goat	1:100	Santa Cruz Biotech.	sc-104661	RRID:AB_2194626
SOMATOSTATIN	Rat	1:100	EMD Millipore	MAB354	RRID:AB_2255365
TBR1	Rabbit	1:2000	Abcam	ab 31940	RRID:AB_2200219
TBR2 (EOMES)	Chicken	1:1000	EMD Millipore	ab15894	RRID:AB_10615604
TIM1 (HAVCR1)	Goat	1:100	R&D Systems	AF1750	RRID:AB_2116561
TYRO3	Mouse	1:50	R&D Systems	FAB859P	RRID:AB_2210976
TYRO3	Goat	1:100	R&D Systems	AF859-SP	RRID:AB_355666
VGLUT1 (SLC17A7)	Guinea Pig	1:1000	EMD Millipore	ab5905	RRID:AB_2301751

DHSB, Developmental Studies Hybdridoma Bank; RRID, Research Resource Identifiers (http://antibodyregistry.org/)

SUPPLEMENTAL EXPERIMENTAL PROCEDURES

Alternative organoid differentiation methods

The differentiation of basal ganglionic eminence (GE) organoids was based upon the methods used for cortical organoid differentiation. From day 15-21, smoothened agonist (SAG, Millipore) was added to the media to activate sonic hedgehog signaling (200 nM for the lateral ganglionic eminence organoid; 1μM for the medial or caudal ganglionic eminence).

Cerebral organoids produced using the Lancaster method in Figure S2 were cultured as described (Lancaster et al., 2013; Lancaster and Knoblich, 2014). Briefly, H9 hESCs cultured on irradiated mouse embryonic fibroblasts were lifted using Dispase and then dissociated to single cells by trypsinization. Cells were plated to Corning low-attachment U-bottomed 96-well plates at 9,000 cells per well in low-bFGF media with Rock inhibitor. Aggregates were fed every other day. On day 6, aggregates were transferred to Corning low-attachment 24-well plates in neural induction media. On day 11, the aggregates were embedded in Matrigel (BD Biosciences) and then grown in differentiation media. After 4 days, Matrigel-coated aggregates were transferred to spinning bioreactors and B27 without Vitamin A was replaced with B27 with Vitamin A and the media was changed weekly.

ZIKV Drug Testing

For CH25H experiments, organoids were pre-treated with 0.1-2.5 μM of CH25H for 12-15 hours, before infection with ZIKV. 2 hours after inoculation, CH25H was added and maintained at 0.1-2.5 μM throughout the experiments. For AXL blocking antibody (100 μg/ml), Duramycin (0.1-1 μM), Azithromycin (5-40 μM), and Ivermectin (0.5 μM) experiments, organoids were pretreated with these compounds for 3 hours prior to ZIKV inoculation, and maintained at described concentrations throughout the experiments. For R428 (30 nM-1 μM), organoids were pretreated for 24 hours, and maintained with the indicated concentration throughout the experiments. For two-dimensional cortical cultures, W6 cerebral organoids were dissociated and plated at 400,000 cells/well in a 24-well plate a day prior to ZIKV infection. Spinal cord progenitors around D21 were differentiated as described. Both neural progenitors were inoculated with viral supernatant and incubated for 2 hours (MOI = 0.8 to 1) before dilution to 1:2 with fresh media. After 24 hours, media was exchanged and cell cultures analyzed at various time points.

Human fetal tissue

Experiments were performed with prior approval from the research ethics committees at the UCLA Office of the Human Research Protection Program and the University of Tubingen (institutional review board [IRB] #323/2017BO2) and Novogenix Laboratories. Embryonic tissues were obtained with informed consent as discarded materials resulting from elective, legal terminations. Samples were de-identified in accordance with institutional guidelines. Specimen ages for this study are denoted as gestational weeks, as determined by the date of the last menstrual period or ultrasound, and confirmed by analysis of developmental characteristics. Samples were processed as described below.

Tissue Processing and Immunohistochemistry

Organoids were fixed in 4% Paraformaldehyde (PFA) in Phosphate Buffered Saline (PBS) for 20 minutes on ice and then washed twice in PBS. Organoids were then incubated in 30% sucrose in PBS for 1-3 hours on ice until completely submersed, embedded, and frozen in Tissue-Tek Optimal Cutting Temperature (O.C.T., Sakura), cryosectioned at 12μm thickness, and collected onto Superfrost Plus slides (Fisher Scientific). GW14-17 human fetal brain tissue was fixed in 4% PFA in PBS for 3-4 days at 4 °C, washed twice in PBS, and immersed in 30% sucrose in PBS overnight at 4 °C. The tissue was then frozen in O.C.T. and cryosectioned at 20 μm thickness. Paraffin embedded GW4 human fetal specimens were prepared at the University of Tübingen, microtome sectioned at by the UCLA Pathology Core, and microtome sectioned at 10 μm thickness by the UCLA Pathology Core. The paraffin embedded tissue was dehydrated and processed for antigen retrieval.

For adherent neural progenitors, cells were fixed in 4% PFA in PBS for 10 minutes on ice and washed twice in PBS. Cells were then permeabilized with PBST for 5 minutes at RT, blocked with 1% HIHS and 0.1% Triton X-100 in PBS for 10 minutes at RT, and incubated with primary antibodies diluted in the blocking solution overnight at 4 °C. Cells were then washed with blocking solution three times for 5 minutes each, and incubated with secondary antibodies and Hoechst 33258 diluted in the blocking solution for 1 hour at RT. After three washes with the blocking solution, cells were mounted in ProLong Diamond Antifade Mountant and imaged using a confocal microscope.

Microscopic imaging
Confocal images were acquired using Zeiss LSM 700, LSM 780, or Zeiss LSM 800 confocal microscopes equipped with a motorized stage and Zen black or blue software. Tiled images were assembled using the Zen Tiles and Positions module. For brightfield imaging, an EVOS microscope (Advanced Microscopy Group) was used. All images were compiled in Adobe Photoshop, with image adjustments applied to the entire image and restricted to brightness, contrast, and levels. Images shown in figures as comparisons were obtained and processed in parallel using identical settings.

Calcium Imaging
For two-photon calcium imaging experiments, AAV1-Synapsin::GCaMP6f adenoviruses (AV-1-PV2822) were obtained from the University of Pennsylvania Vector Core (https://www.med.upenn.edu/gtp/vectorcore/). Organoids were inoculated with 1:50 diluted viral stocks overnight and replaced with fresh media after 12-17 hours. After 7-14 days, organoids were mounted in collagen or Matrigel without phenol red in N2B27 media containing BrainPhys Neuronal Media (Stem Cell Technologies) as the base media instead of DMEM/F12.

Calcium imaging was performed using a resonant scanning two-photon microscope (Scientifica) equipped with a Ti:sapphire excitation laser (Coherent, Ultra 2), operated at 920 nm. Images with approximately 500 µm x 500 µm field-of-view were acquired at a frame rate of 30.9 Hz using a 20x 0.8 NA objective. Raw calcium imaging movies were processed in MATLAB using custom-written analysis scripts. Motion corrections of small horizontal drifts were performed with a recursive image registration algorithm. The same algorithm was used to align and concatenate videos of two consecutive recording sessions. Active neurons were detected with an automated segmentation algorithm (Cai et al., 2016) which (i) detected 'bright pixels' of local fluorescence maxima meeting minimum fluorescence criteria and (ii) used an iterative process to group together neighboring pixels based on the correlation of each bright pixel's fluorescence time trace (±20s window around local maxima of fluorescence event) with the mean time trace of the pixels group in the previous iterative step. Pixels with correlation > 0.35 were added to the group, and the process was repeated until the total number of pixels in the group no longer changed. Cells whose centroids were within 2 µm of each other or whose pixels overlapped by at least 70%, were merged together. Segments with eccentricity > 98% were discarded to avoid elongated dendritic and axonal structures. ΔF/F traces were calculated for each segment by computing the average fluorescence value F(t) over all pixels at each time point, and then subtracting the cell's mode value over the whole video and dividing by the same number. Traces were low pass-filtered using a 10-th order Butterworth filter with 5Hz cutoff frequency. Finally, all detected segments and ΔF/F traces were examined visually, and only segments corresponding to neuronal somas with clear fluorescence peaks, were analyzed further. Putative spikes were extracted by deconvolving the ΔF/F traces with a 2 s single-exponential kernel (Yaksi and Friedrich, 2006) and applying a spike detection threshold of 2.5x standard deviation of the deconvolved trace. Spike rates were computed for each cell, over 0.33 sec-long bins, overlapping by 50%.

Pearson's Correlation coefficients were computed between all pairs of firing rates vectors. To detect significantly correlated cell pairs, we circularly shifted the firing rate vector of each cell by a random lag (up to half the movie duration), while keeping that of the second cell unaltered, and computed the new correlation between the two traces. This was repeated 1000 times for each of the two cells in a pair, yielding a distribution of 2000 'shifted-correlation' values. A cell pair was significantly correlated if its default correlation exceeded the 95th percentile of the shifted-correlation distribution.

Electrophysiology
Organoids were embedded in 4% low gelling agarose (Sigma) cooled to 47 °C and sliced in artificial cerebrospinal fluid (aCSF) containing 125 mM NaCl, 2.5m M KCl, 1 mM $MgCl_2 \cdot 6H_2O$, 2 mM $CaCl_2 \cdot 2H_2O$, 1.25 mM $NaH_2PO_4 \cdot H_2O$, 25 mM $NaHCO_3$, and 0.45% glucose using a vibratome (Leica VT1000S) at 200-250 µm thickness. aCSF was oxygenated (95% O_2/5% CO_2) to pH of 7.4 and cooled on ice during the slice preparation. Slices were cultured on Millicell membrane (Millicell Cell Culture Insert, 0.4 µm, 30 mm diameter, ref# PICM0RG50, Millipore) in N2B27 media at 40% O_2 for up to one week before recording.

Cells were visualized with infrared optics on an upright microscope (BX51WI, Olympus). pCLAMP10 software and a MultiClamp 700B amplifier was used for electrophysiology (Axon Instruments). The aCSF contained the following: 124 mM NaCl, 4.5 mM KCl, 2 mM $CaCl_2$, 1 mM $MgCl_2$, 26 mM $NaHCO_3$, 1.2 mM NaH_2PO_4, and 10

mM D-glucose continuously bubbled with a mixture of 95% O_2/5% CO_2. The intracellular solution in the patch pipette comprised the following: 135 mM potassium gluconate, 3 mM KCl, 0.1 mM $CaCl_2$, 10 mM HEPES, 1 mM EGTA, 8 mM Na_2-phosphocreatine, 4 mM Mg-ATP, 0.3 mM Na_2-GTP; pH 7.3 adjusted with KOH. The patch-pipettes had 5–6 MΩ resistance when filled with intracellular solution. The tip potential of -15.6 mV was corrected in all the data that are shown. The data were analyzed with Clampfit10.2 (Molecular Devices). All statistical tests were run in GraphPad InStat 3. The graphs were created in GraphPad Prism and assembled in Adobe Illustrator. N numbers are defined as the numbers of cells defined in the figure legends.

RNA Isolation, Processing, Microarray Hybridization, RNA-Sequencing, and Transcriptome Analyses

Human cortical organoids were lysed in QIAzol reagents and RNA was extracted following manufacturer's instructions (miRNeasy Micro Kit, Qiagen). For CoNTExT, TMAP, WGCNA, and GO ontology analyses (Figure 2), cerebral organoids derived from H9 were collected with 3 replicates (3 independent experiments, 12 samples total) at W5, W8, W11, and W14 and RNA samples were sent to the UCLA Neuroscience Genomics Core. RNA integrity was confirmed with the Agilent 2100 Bioanalyzer (RIN > 8) and samples were hybridized to the HumanHT 12v4.0. Expression data was analyzed as described in Stein et al., 2014 and are publicly available. For ZIKV analyses (Figure 6), W8 mock and ZIKV infected cerebral organoids 3 and 5 days post infection were collected with 3 replicates (6 samples total). RNA samples were sent to the UCLA Clinical Microarray Core (CMC) and RNA integrity was confirmed with the Agilent 2100 Bioanalyzer. The cDNA libraries were generated using the KAPA stranded mRNA-Seq kits (KAPA Biosystems) and sequenced using Illumina HiSeq 3000, yielding between 27 and 101 million reads per sample. Quality control was performed on base qualities and nucleotide composition of sequences. Alignment to the human genome (hg38) was performed using the STAR spliced read aligner (Dobin et al., 2013) with default parameters. Additional QC was performed after the alignment to examine: the level of mismatch rate, mapping rate to the whole genome, repeats, chromosomes, key transcriptomic regions (exons, introns, UTRs, genes), insert sizes, AT/GC dropout, transcript coverage and GC bias. One sample (a 3-day control sample) resulted an outlier and was excluded from further analysis. Between 84 and 89% (average 86%) of the reads mapped uniquely to the human genome. Total counts of read-fragments aligned to candidate gene regions were derived using HTSeq program (www.huber.embl.de/users/anders/HTSeq/doc/overview.html) with *H. Sapiens* hg38 refSeq (refFlat table) as a reference and used as a basis for the quantification of gene expression. Only uniquely mapped reads were used for subsequent analyses. Differential expression analysis was conducted with R-project and the Bioconductor package Limma-voom (Law et al., 2014) Statistical significance of the differential expression was determined at false discovery rate (FDR) < 5%. Differentially regulated genes were assigned to relevant Gene Ontology groups using Metascape online software (http://metascape.org) (Tripathi et al., 2015).

Quantitative PCR

Reverse Transcriptase qPCR (RT-qPCR) was performed as described (Kong et al., 2015). In brief, total RNA was extracted with either an RNeasy Mini or miRNeasy Mini Kit (Qiagen). For each sample, >500 ng of total RNA was used for cDNA synthesis using the SuperScript IV First-Strand Synthesis System (Invitrogen). In each RT-qPCR reaction, cDNA was combined with LightCycler 480 SYBR Green I Master Mix (Roche) and the exon-spanning primer pairs listed below. All primer pairs were validated for ≥ 1.8 amplification efficiency as previously described (Watanabe et al., 2012). All samples were run using a Roche LightCycler 480 real-time PCR system in duplicates, and relative expression levels determined by normalizing the crossing points to the internal reference gene *ACTB* (β-Actin). Primers used are as follows: β-ACTIN (Amplicon size 200bp) fw 5'-CTGTGGCATCCACGAAACTA-3' rv 5'-AGTACTTGCGCTCAGGAGGA-3': FOXG1 (Amplicon size 191bp) fw 5'-CCAGACCAGTTACTTTTTCCC-3' rv 5'-TGAAATAATCAGACAGTCCCCC-3': GAD65 (Amplicon size 140bp) fw 5'-TTTTGGTCTTTCGGGTCGGAA-3' rv 5'-TTCTCGGCGTCTCCGTAGAG-3': GFAP (Amplicon size 209bp) fw 5'-CTGCGGCTCGATCAACTCA-3' rv 5'-TCCAGCGACTCAATCTTCCTC-3': GSX2 (Amplicon size 106bp) fw 5'-ATGTCGCGCTCCTTCTATGTC-3' rv 5'-CAAGCGGGATGAAGAAATCCG-3': NKX2.1 (Amplicon size 68bp) fw 5'-AGCACACGACTCCGTTCTC-3' rv 5'-GCCCACTTTCTTGTAGCTTTCC-3': OLIG2 (Amplicon size 90bp) fw 5'-ATAGATCGACGCGACACCAG-3' rv 5'-ACCCGAAAATCTGGATGCGA-3': PV (Amplicon size 96bp) fw 5'-AAGAGTGCGGATGATGTGAAG-3' rv 5'-GCCTTTTAGGATGAATCCCAGC-3': SST (Amplicon size 108bp) fw 5'-ACCCAACCAGACGGAGAATGA-3' rv 5'-GCCGGGTTTGAGTTAGCAGA-3': ZIKV (Amplicon size 141bp) fw 5'-TTGTGGAAGGTATGTCAGGTG-3' rv 5'-ATCTTACCTCCGCCATGTTG-3'

Statistical analysis

The normality and equality of variance of each data set was determined using GraphPad InStat or Prism software, and appropriate parametric (for normal distributions) or non-parametric (for uneven distributions) were accordingly applied as indicated in the figure legends. Paired and unpaired Student's two tailed *t* tests with or without Welch's correction (as appropriate) and two tailed Mann–Whitney tests were calculated using Prism software. Significance was assumed when $p < 0.05$. Throughout the manuscript, the results of statistical tests (*p* values and n numbers) are reported in the figure legends, Table S4-S5, and asterisks on the panels. Signifiers used are as follows: no significance (n.s.) $p > 0.05$, * $p \leq 0.05$, ** $p \leq 0.01$, *** $p \leq 0.001$, **** $p \leq 0.0001$. All data are presented as mean ± SEM unless otherwise specified in the figure legends.

Immunohistochemistry Quantification

All cell counts and measurements were compiled in Adobe Photoshop and ImageJ. For cerebral induction efficiency (Figure 1B), the percent of total cells double positive for FOXG1 and LHX2 were counted. To exclude the necrotic center of the aggregate, clCASP3$^+$ regions were excluded from the counts. For perimeter analysis in Figure 1C, the perimeters of 3 representative W2.5 organoids were measured across 9 independent experiments using ImageJ. For cell fate quantifications in Figure 1E and 1G, the average number of cells positive for PAX6, SOX2, TBR2, and CTIP2 per field was counted. In Figure S1G, the average percent of cerebral organoid cells positive for SOX2, TBR2, and TBR1 per field was counted. In Figure S1D and S1J, the thickness of the VZ, defined as the SOX2$^+$ dense region, SVZ, defined as the SOX2$^+$ sparse and TBR2$^+$ region, and CP, defined as the dense CTIP2$^+$ regions were measured. In figure S2B, n=8 LAN and n=9 B27 organoids were scored for the number of rosettes with PAX6$^+$ regions; the area and perimeter of the PAX6$^+$ region was measured using ImageJ. n=8 LAN, n=9 B27 organoids were scored. In Figure S3D, the percentage of NKX2.1 positive cells out of total cells per entire W5 organoid were counted. Necrotic cells in the center of the organoids were excluded from cell counts. In Figures 3D and S4B-S4C, quantification of cells per field was measured. Distinctions between VZ and SVZ for thickness measurements were defined as where PAX6 positive cells became less dense and where TBR2 positive cells accumulated. aRG cells were operationally defined as PAX6/pVIM positive cells dividing at the apical membrane; bRG cells were defined as PAX6/pVIM double positive cells dividing outside the VZ. In Figure S5A and S5C, the number of HepaCAM positive astrocytes was represented as the average number of cells positive for HepaCAM per field. In Figures 3H and S4E, the relative distribution of neurons per field of the cortical plate was counted. The apical edge of the CP was assigned a relative positional value of 0 and the basal edge assigned a positional value of 1.0. Median cell positions ± 95% confidence intervals are plotted. In Figure S6B, viral infection efficiency was quantified by scoring the total number of cells expressing GFP, adeno-associated virus AAV1-SYNAPSIN::GCaMP6f, and/or CTIP2. For the cerebral organoids or 2D progenitors infected with ZIKV (Figures 5D, 5H; Figures 6B; Figures S5D, S5E), cells positive for ZIKV, cell specific markers SOX2, TBR2, CTIP2, LHX2, OLIG2, or ISL1, and cell death marker clCASP3 were counted and represented as percentage of all cells surveyed. To measure organoid cell death and size two weeks after ZIKV infection (Fig. 5F), cerebral organoids were stained with 25 µg/ml propidium iodide (PI) and 5 µg/ml Hoechst 33258 at RT for 5 minutes, washed with PBS five times, and then fixed in 4% PFA in PBS for 20 minutes on ice. Organoids were then washed with PBS five times, and placed individually into wells of a 384-well plate (VWR, Greiner bio-one Cat#89047-270) for imaging and size analysis. Images were taken using ImageXpress XL and analyzed using ImageXpress analysis software to measure PI and Hoechst intensity, organoid area, and organoid perimeter.

SUPPLEMENTAL REFERENCES

Cai, D.J., Aharoni, D., Shuman, T., Shobe, J., Biane, J., Song, W., Wei, B., Veshkini, M., La-Vu, M., Lou, J.*, et al.* (2016). A shared neural ensemble links distinct contextual memories encoded close in time. Nature *534*, 115-118.

Diaz Perez, S.V., Kim, R., Li, Z., Marquez, V.E., Patel, S., Plath, K., and Clark, A.T. (2012). Derivation of new human embryonic stem cell lines reveals rapid epigenetic progression in vitro that can be prevented by chemical modification of chromatin. Hum Mol Genet *21*, 751-764.

Dobin, A., Davis, C.A., Schlesinger, F., Drenkow, J., Zaleski, C., Jha, S., Batut, P., Chaisson, M., and Gingeras, T.R. (2013). STAR: ultrafast universal RNA-seq aligner. Bioinformatics *29*, 15-21.

Karumbayaram, S., Lee, P., Azghadi, S.F., Cooper, A.R., Patterson, M., Kohn, D.B., Pyle, A., Clark, A., Byrne, J., Zack, J.A.*, et al.* (2012). From skin biopsy to neurons through a pluripotent intermediate under Good Manufacturing Practice protocols. Stem Cells Transl Med *1*, 36-43.

Kong, J.H., Yang, L., Dessaud, E., Chuang, K., Moore, D.M., Rohatgi, R., Briscoe, J., and Novitch, B.G. (2015). Notch activity modulates the responsiveness of neural progenitors to sonic hedgehog signaling. Developmental cell *33*, 373-387.

Lancaster, M.A., and Knoblich, J.A. (2014). Generation of cerebral organoids from human pluripotent stem cells. Nat Protoc *9*, 2329-2340.

Lancaster, M.A., Renner, M., Martin, C.A., Wenzel, D., Bicknell, L.S., Hurles, M.E., Homfray, T., Penninger, J.M., Jackson, A.P., and Knoblich, J.A. (2013). Cerebral organoids model human brain development and microcephaly. Nature *501*, 373-379.

Law, C.W., Chen, Y., Shi, W., and Smyth, G.K. (2014). Voom: precision weights unlock linear model analysis tools for RNA-seq read counts. Genome biology *15*, R29.

Lowry, W.E., Richter, L., Yachechko, R., Pyle, A.D., Tchieu, J., Sridharan, R., Clark, A.T., and Plath, K. (2008). Generation of human induced pluripotent stem cells from dermal fibroblasts. Proc Natl Acad Sci U S A *105*, 2883-2888.

Robinson, M.D., McCarthy, D.J., and Smyth, G.K. (2010). edgeR: a Bioconductor package for differential expression analysis of digital gene expression data. Bioinformatics 26, 139-140.

Schneider, C.A., Rasband, W.S., and Eliceiri, K.W. (2012). NIH Image to ImageJ: 25 years of image analysis. Nat Methods 9, 671-675.

Thomson, J.A., Itskovitz-Eldor, J., Shapiro, S.S., Waknitz, M.A., Swiergiel, J.J., Marshall, V.S., and Jones, J.M. (1998). Embryonic stem cell lines derived from human blastocysts. Science 282, 1145-1147.

Tripathi, S., Pohl, M.O., Zhou, Y., Rodriguez-Frandsen, A., Wang, G., Stein, D.A., Moulton, H.M., DeJesus, P., Che, J., Mulder, L.C.*, et al.* (2015). Meta- and Orthogonal Integration of Influenza "OMICs" Data Defines a Role for UBR4 in Virus Budding. Cell Host Microbe *18*, 723-735.

Watanabe, M., Kang, Y.-J., Davies, L.M., Meghpara, S., Lau, K., Chung, C.-Y., Kathiriya, J., Hadjantonakis, A.-K., and Monuki, E.S. (2012). BMP4 sufficiency to induce choroid plexus epithelial fate from embryonic stem cell-derived neuroepithelial progenitors. Journal of Neuroscience *32*, 15934-15945.

Yaksi, E., and Friedrich, R.W. (2006). Reconstruction of firing rate changes across neuronal populations by temporally deconvolved Ca2+ imaging. Nat Methods *3*, 377-383.